IOP Publishing Smart Materials and Structures
Smart Mater. Struct. **24** (2015) 065014 (11pp) doi:10.1088/0964-1726/24/6/065014

Sensitivity and directionality of lipid bilayer mechanotransduction studied using a revised, highly durable membrane-based hair cell sensor

Nima Tamaddoni[1], **Eric C Freeman**[2] **and Stephen A Sarles**[1]

[1] Department of Mechanical, Aerospace and Biomedical Engineering, University of Tennessee, Knoxville, TN, 37996, USA
[2] College of Engineering, University of Georgia, Athens, GA 30602, USA

E-mail: ssarles@utk.edu

Received 2 November 2014, revised 3 March 2015
Accepted for publication 4 March 2015
Published 7 May 2015

Abstract

A bioinspired, membrane-based hair cell sensor consists of a planar lipid bilayer formed between two lipid-coated water droplets that connect to an artificial hair. This assembly enables motion of the hair caused by mechanical stimuli to vibrate the bilayer and produce a capacitive current. In this work, the mechanoelectrical transduction mechanism and sensing performance is experimentally characterized for a more-durable, revised hair cell embodiment that includes a cantilevered hair rooted firmly in the surrounding solid substrate. Specifically, this study demonstrates that the revised membrane-based hair cell sensor produces higher time rates of change in capacitance (0.8–6.0 nF s^{-1}) in response to airflow across the hair compared to the original sensor (45–60 pF s^{-1}) that did not feature a cantilevered hair. The 10-fold to 100-fold increase in the time rate change of capacitance corresponds to greater membrane bending and, thus, higher sensing currents. Membranes in the revised sensor exhibit changes in area due to bending on the order of 0.2–2.0%, versus 0.02% for the original sensor. Experiments also reveal that the bilayer displays highest sensitivity to mechanical perturbations normal to the plane of the bilayer, a membrane can transduce hair motion at frequencies below the hair's characteristic frequency, and bilayers formed between polymerized hydrogel volumes exhibit a higher sensing currents than those formed between liquid aqueous volumes. Finally, measurements of sensitivity (5–35 pA m^{-1} s^{-1}) and minimum (4.0–0.6 m s^{-1}) and maximum (28–13 m s^{-1}) sensing thresholds to airflow are performed for the first time, and we observe maximum electrical power (~65 pW) in the membrane occurs for combinations of slower airflow and higher voltage. These results highlight that along with the dimensions of the hair and the compositions of the aqueous volumes, sensing performance can be tuned with applied voltage.

S Online supplementary data available from stacks.iop.org/SMS/24/065014/mmedia

Keywords: droplet interface bilayer, membrane-based hair cell sensor, mechanotransduction, airflow, sensitivity, directionality, electrical power

(Some figures may appear in colour only in the online journal)

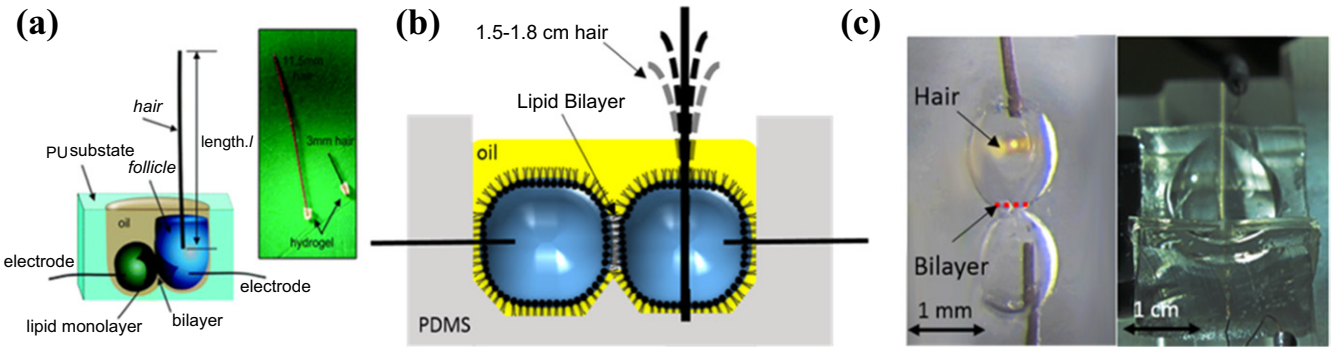

Figure 1. (a) Original hair cell sensor reprinted with permission [1]. (b) Schematic of revised hair cell embodiment (not to scale). (c) A top view (left) and isometric view (right) of the revised hair cell sensor.

1. Introduction

Nature's hair cell structures, including those used for hearing [2, 3], tactility [4], and flow measurement [5], have inspired the development of many engineered devices in the last decade. All of these bio-inspired designs employ an artificial hair structure for mechanical sensing or actuation. Examples include an airflow velocity sensor [6, 7], an oscillating flow sensor [8], a magnetostrictive force sensor [9], a microparticle actuator [10], and an underwater directional flow sensor [7, 11, 12]. One significant difference between these man-made designs and natural hair cells is the use of engineered transducers (i.e. cantilever beams and solid materials) in place of biomolecules to perform transduction.

Motivated to construct a biomolecular hair cell sensor, Sarles and Leo combined phospholipid self-assembly methods with soft materials to create a transducer whose sensing element is an artificial cell membrane, or lipid bilayer [1]. This membrane-based hair cell is responsive to mechanical perturbation of a hair that induces oscillation in the bilayer, which generates a measurable current due to the time rate of change of electrical capacitance of the vibrating membrane [1]. This transduction process was verified by observing that the sensing current is proportional to the voltage applied across the lipid bilayer membrane [1]. In that study, perturbation of the hair with airflow resulted in measured currents on the order of 10–100 pA [1].

Although the first embodiment produced a sufficient time rate of change in capacitance and thus a measurable signal for exploring bilayer-based transduction of hair motion, the sensor exhibited several limitations. These include low mechanical stability of the hair that was supported only by a small hydrogel volume, poor membrane durability due to excessive hair motion, low sensitivity, and undefined directionality. The goal in our current work is to revise the sensor design and fabrication methods to establish a well-supported hair cell structure with improved stability of the hair and greater bilayer durability, as well as an increased operating range. In addition, we are motivated to achieve a more durable embodiment to be able to thoroughly investigate and characterize the directionality and sensitivity of the device. With more durable sensors and better understanding of the sensing mechanism and operational limits, we aim to construct arrays for providing distributed sensing and increased directionality. Such arrays of natural hair cells are common in organisms and are known to provide sensing robustness, sensitivity, frequency selectivity, directionality, and spatial awareness [13–16].

In this work, we present and characterize a revised version of the membrane-based hair cell sensor that utilizes a cantilevered hair, rooted at its base within the polymeric encapsulating substrate. It is shown that this adjustment yields significantly greater mechanical stability for the hair structure and increased bilayer durability by preventing the hair from falling over and rupturing the bilayer. Similar to the previous effort [1], the hair passes through one of two lipid-coated aqueous volumes submerged in oil; the phospholipid-coated volumes connect to form a 5 nm thick unilamellar membrane lipid bilayer. Oscillation of the hair transmits energy to the bilayer, resulting in a measurable current produced by the time rate of change of electrical capacitance of the vibrating membrane [1]. The first target of our study is to experimentally characterize the perturbation-induced current response of the lipid bilayer due to vibration of the modified hair support. Three types of perturbation are utilized to characterize the device: steady airflow, direct oscillation of the hair by a mechanical shaker, and periodic free displacement of the hair using an automated flicking device. Because of enhanced sensor durability, we also perform several experiments that add to our understanding of the mechanotransduction process and sensing performance for a membrane-based hair cell sensor. Specifically, we measure the directional response of a membrane-based hair cell sensor for the first time, examine its response to low frequency excitation (below the first resonance frequency of the hair), and study the effects of using liquids versus gel materials for the aqueous volumes. Finally, we quantify the sensitivity, minimum sensing threshold, and the dynamic range of the sensor in response to airflow across the hair.

2. Revised embodiment of the sensor

A schematic of the original membrane-based hair cell is shown in figure 1(a). In the original version, the hair is rooted in a small volume (~1 μl) of hydrogel that comprises one of the two lipid-coated aqueous volumes residing in the oil-filled

substrate [1]. In practice, this method for supporting the hair and the aqueous droplets limits durability as intense stimuli causes the hair to fall over and rupture the bilayer. Membrane rupture is also possible if the supporting gel volume rotates within the compartment of the substrate. This variation of contact with the other droplet may also affect the directionality and reproducibility of the sensing response even if the membrane survives the gel's motion. Additionally, the volume of each droplet is different since one droplet is supplemented with gel and polymerized in a separate step before forming a bilayer. The dissimilar aqueous volumes (i.e. one solid and one liquid) can cause unbalanced energy transfer to the membrane from each side. Furthermore, inconsistent positioning of the hydrogel volume or hair within the compartment may also cause problems in maintaining contact with the wire-type electrodes needed to extract sensing current.

The revised hair cell sensor embodiment shown schematically in figure 1(b) features a hair structure that is rooted into the polymeric substrate at the bottom of the droplet compartment for increased durability and mechanical stability. Similar to the previous work, the hair is made from a paintbrush fiber with diameter of 90–110 μm. Inserting 1–2 mm of the length of the hair into the substrate has multiple advantages: (1) the hair remains fixed in place even during high levels of mechanical perturbation; and (2) either hydrogel or liquid may be used to comprise the aqueous volume that surrounds the hair, since the substrate maintains the hair's orientation. The latter means that symmetric compositions of aqueous volumes can be chosen to construct the sensor, and the volumes are expected to maintain more consistent contact during perturbation because the position of the base of the hair remains fixed. However, this change in boundary conditions may also affect the characteristic frequency of vibration of the hair as well as the force transmissibility of hair motion to the lipid membrane.

In the following results and discussion section, we present new experimental results that confirm that this change in boundary conditions significantly enhances the durability of the sensor. Consequently, additional tests are performed in this study to characterize the mechanoelectrical transduction response of the revised embodiment for both liquid and gel-phase aqueous volumes, and the directionality, low-frequency response, and sensing performance are experimentally measured for the first time.

3. Materials and methods

3.1. Substrate fabrication

A flexible polydimethylsiloxane (PDMS, *Sylgard* 184, *Dow Corning*) substrate is used to hold the liquid volumes and the hair. The substrate allows control of the size of bilayer [17], prevents leaking of the liquids, and supports the electrodes that are required for electrical interrogation and stimulation of the bilayer. PDMS substrates are fabricated through a double molding step and silver–silver chloride wire-type electrodes (125 μm diameter) are prepared and inserted into the substrate as described elsewhere [1, 17]. The polymeric fiber (90–110 μm diameter) used as the hair is obtained from a Prostroke 101B paintbrush. A hole for rooting the hair is created in the PDMS substrate in the center of one of the droplet compartments by piercing from the bottom with a 150 μm diameter drill bit. The hair is then inserted through the pierced hole from the top (figure 1(b)), such that it will pass through the center of one of the aqueous volumes. The hair can be inserted either before or after a droplet is dispensed into the compartment. We examined the effect of varying the depth of fixation in the substrate and found that deeper hair insertion leads to increased vibration of the substrate that results in greater background current due to the vibration of the electrodes when the hair is perturbed. Thus, the hair is inserted ca. 1–2 mm into the PDMS substrate. The remaining free length of the hair is 16–18 mm, measured vertically from the bottom of the compartment to the tip of the hair. This configuration is used in all measurements performed; figure 1(c) shows images of the sensor from top and isometric perspectives. Images of assembled hair cell sensors are obtained through the Leica M80 stereomicroscope using a Canon G12 digital camera.

3.2. Materials

Lipid bilayers are formed at the interface of lipid-coated aqueous volumes consisting of either an aqueous liposome suspension (liquid) or a mixture of liposomes and a photopolymerizable hydrophilic polymer (hydrogel) in aqueous buffer. Aqueous liposome solution containing 2 mg ml^{-1} of 1, 2-diphytanoyl-sn-glycero-3-phosphocholine (DPhPC, Avanti Polar Lipids, Inc.) liposomes in 200 mM NaCl, 10 mM, 4-morpholinepropanesulfonic acid (MOPS), pH7 is prepared as described by Hwang *et al* [18]. Difunctional poly(ethylene glycol) diacrylate (PEGDA, 6000 g mole^{-1}, Sigma) was obtained and used without further purification. A stock PEGDA solution is prepared by dissolving PEGDA (20% w/v) and Irgacure 2959 (BASF) photoinitiator (0.1% w/v) into deionized water and the mixture is poured into a ultraviolet (UV) protected bottle at 4 °C. The gel stock solution is stored at −20 °C until needed when it is combined with the stock liposome solution at a 1:1 (v/v) ratio to yield a final gel-lipid mixture consisting of 10% (w/v) PEGDA, 0.05% (w/v) Irgacure 2959, and 1 mg ml^{-1} DPhPC vesicles in 100 mM NaCl, 5 mM MOPS, pH 7. Hexadecane (Sigma, >99%) is used as the oil in all experiments.

3.3. Bilayer formation and hydrogel polymerization

An interfacial lipid bilayer is formed between lipid-encased aqueous volumes (liposome solution or PEG–lipid mixture) contained in the neighboring compartments of the PDMS substrate. Positioning and attachment of the lipid-coated volumes in the substrate is performed via the regulated attachment method [17]. Reducing compression on the substrate to open the dividing aperture between compartments allows the droplets to come into contact, after which a lipid

bilayer spontaneously forms at the interface of the two lipid-encased volumes. The final area of the bilayer is controlled by adjusting the width of the aperture between compartments via lateral compression of the substrate using a manual micromanipulator (KITE-R, World Precision Instruments). Bilayers created between droplets in hexadecane typically form within 2–3 min after contact. Following membrane assembly, PEG–lipid volumes are photopolymerized under UV light for 9 min using a LED-200 portable light (Electro-Lite Corp) with a power output of 2.5 W cm^{-2} at 365 nm. Electrical measurements confirm that the bilayer remains stable during photopolymerization of gel volumes [19].

3.4. Electrical recording of bilayer formation

Bilayer characterization and hair cell sensor measurements are performed within a grounded Faraday cage where the noise level of measured current is ca. ±1–3 pA. During bilayer formation, current measurements are performed using an AxoPatch200B patch clamp amplifier and Digidata 1440A data acquisition system (Molecular Devices) to measure the resulting capacitive square-wave current induced by an externally generated 10 mV, 10 Hz triangular voltage waveform. The triangle wave voltage is generated using an Agilent 33210A function generator. Prior to any testing of the mechanoelectrical response, the area of each DPhPC bilayer is adjusted to 0.042 mm^2 by varying substrate compression until the square wave current through the bilayer has an amplitude of 100 pA.

3.5. Perturbation techniques and measurement of sensor response

The sensing response of the revised hair cell is characterized using three forms of mechanical perturbation to the hair. In the first case, a horizontal steady airflow exiting a 0.61 mm inner diameter needle tube at a distance 4–5 mm from the hair is applied at varying flow velocities to perturb the hair. A tank of compressed nitrogen is used as the source for airflow, and pressure is controlled with a two-stage regulator. Pneumatic tubing and push-to-connect fittings are used to connect the tank to the needle fixture. Flow velocities ranging from 3 to 20 m s^{-1} at the hair location are calibrated to the regulated pressure using an anemometer (Multi-Function Instruments, model: TA 465). Second, a mechanical shaker (PASCO, SF-9324) is connected to an aluminum rod that attaches to the hair using beeswax to shake the hair at known frequency. Third, an automated flicker consisting of a servomotor and rotating plastic wand is used to induce free vibration of the hair by bending and releasing the hair as the wand rotates. The flicker impacts the hair at a distance of 1–2 mm from the free end (top).

Sensing current generated by the lipid bilayer is low-pass filtered at 2 kHz and sampled at 20 kHz using the AxoPatch200B and Digidata 1440A with data analysis performed using MATLAB. A power spectral density (PSD) using Welch's method of the current response is performed to determine the average power as a function of frequency for the measured signal. Additionally, a FASTCAM 1024 PCI high-speed camera is used to track the motion of the tip of the hair during free vibration after flicking. The camera is positioned above the sensor and captures hair motion from a top view at 6000 frames per second. Images are saved in '.tiff' format. The tip position of the hair is projected on a 2D plane for plotting, and the frequency of the hair oscillation is obtained from tip position versus time data by calculating the PSD in MATLAB.

4. Results and discussion

One of the limitations of the first membrane-based hair cell sensor was low stability and bilayer durability. In this work, we revised the design by rooting the hair into the polymeric substrate so that the hair does not fall and that it resumes its original orientation after perturbation ends. To characterize the durability, we subjected the revised embodiment to two types of stimuli: repeated-flicking and continuous airflow (see supporting information). These tests reveal that the modified design of the sensor allows the bilayer to remain intact under significant (and repeated) deflections of the hair (figures S1(a) and (b)) and during long periods of continuous perturbation (figures S1(c) and (d)). These data also highlight that it is possible to subject the revised sensor to airflow speeds up to 28 m s^{-1} (10 kPa) whereas the previous version of the hair cell could only withstand airflow up to 5 kPa, even with a larger output tube diameter (i.e. lower speed) [1].

As a result of the enhanced stability, we are motivated to conduct a thorough study of the mechanoelectrical response of a bilayer-based hair cell subjected to multiple types of perturbation. This assessment is especially important since the boundary condition of the supported hair has changed in the revised sensor embodiment and because hydrogel material is not required in the aqueous volumes. These studies primarily utilize lipid bilayers formed with liquid aqueous volumes, except where noted otherwise.

4.1. Characterization of mechanoelectrical sensing response

Previous research demonstrated that the capacitive sensing current in response to airflow is voltage dependent [1]. Specifically, the current generated by the membrane depends on both the time to the third power of voltage, V, because the capacitance of the bilayer, C, itself follows a linear trend with respect to V^2 due to electrowetting. The expression for sensing current, $i(t)$, is given by

$$i(t) = \frac{\mathrm{d}C}{\mathrm{d}t}\left(V + \alpha V^3\right) + i_{v=0}, \tag{1}$$

where α is the electrowetting constant for the two monolayers that comprise the membrane and $\mathrm{d}C/\mathrm{d}t$ is the time rate of change of bilayer capacitance induced by mechanical perturbation of the hair. The relationship also includes the term, $i_{v=0}$, which represents the current produced by mechanical vibration of the positive electrode [20]. The subscript $v = 0$ is used to denote that this background current

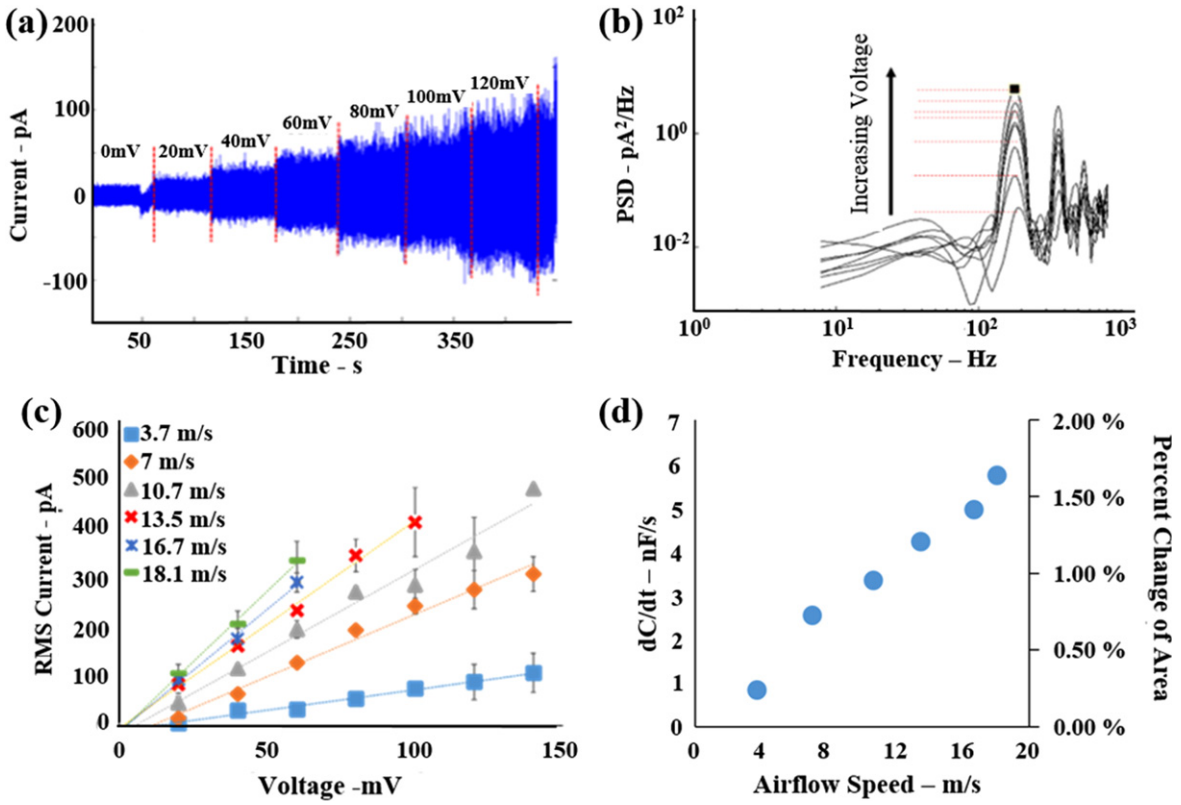

Figure 2. (a) The current response at different voltages for an airflow speed of 7 m s^{-1}. (b) Power spectral density of current at different voltages for airflow at 7 m s^{-1}. (c) Rms current versus voltage at different airflow speeds. (d) Time rate change of bilayer capacitance (left axis) and the percent area change (right axis) for different airflow speeds.

is non-capacitive, and, hence, it does not vary with the applied voltage. As a result, the amplitude of the sensing current increases with respect to the rate change of capacitance due to membrane vibration and the increase in capacitance due to electrowetting by the two droplets.

4.1.1. Quantification of the time rate change of membrane capacitance. The purpose of the first part of the study is to quantify the time rate of change in capacitance of the membrane, d*C*/d*t*, which provides a measure of how much the bilayer vibrates in response to perturbation of the hair, across a wider range of stimuli strength. To do so, a series of experiments were performed at varying airflow speeds. Airflow was applied to the hair cell in a direction perpendicular to the bilayer in all cases. At each flow speed, the current produced by the bilayer was measured for 20 s at applied transmembrane voltages from 0 to +140 mV in 20 mV steps. Figure 2(a) shows the raw current response to continuous airflow at 7 m s^{-1} applied, and the increases in current correspond to stepwise increases in the applied dc voltage. At each voltage level, the tip of the hair exhibits a net deflection of ca. 1 mm, about which it vibrates in the airflow. Since the airflow exits a small, 0.6 mm diameter needle, it is likely the hair moves in and out of the flow path during excitation. Under steady airflow, the current at each voltage exhibits two primary resonances (180 and 360 Hz) as shown in the PSDs in figure 2(b). The amplitude of the PSD at resonance increases with the amplitude of the applied voltage. This result confirms that the membrane produces a capacitive current and that the frequency of oscillation is independent of the applied voltage level. Separately, measurements at different airflow speeds also confirm that the frequency of the current oscillation is independent of the airflow speed, indicating that the membrane vibrates at a constant speed regardless of the airflow strength. The fact that the peak frequency of the current of all airflow speeds matches the natural frequency of the hair, as determined by high speed imaging (see supporting information), confirms that the hair vibrates at its natural frequency at all speeds tested. The second harmonic in the PSD analysis (figure 2(b)), which is also voltage dependent, indicates that the membrane also vibrates at the first harmonic of the hair's fundamental frequency.

Figure 2(c) shows rms values of the measured current versus applied voltage for six different flow speeds from ~4 to 18 m s^{-1}. Each data point in this figure represents the average of the rms current measured for three different bilayers formed in the same substrate and tested with the same hair at each voltage and speed. The measured current at zero volts during the airflow has been subtracted from each of the averaged current values to remove background current ($i_{v=0}$) not associated with membrane vibration. In addition, the areas of the bilayers were held constant at ca. 0.042 mm^2 at every voltage level by using the regulated attachment technique [17] to return the bilayer area to its zero-voltage value. This correction was applied to eliminate changes in area of the

bilayer due to the electrowetting effect (i.e. $\alpha = 0$) [1]. Consequently, the data show linear relationships between rms current versus voltage for the various airflow speeds, where the slope of each current–voltage series represents the time rate of change of membrane capacitance, dC/dt, at each airflow speed. More generally, the data show that lower airflow speeds produce less current per unit voltage, while faster airflow induces higher current output due to greater deflection of the hair.

Figure 2(d) shows a plot of the rms time rate of change of capacitance versus airflow speed taken from the current–voltage series in figure 2(c). This presentation shows clearly that the time rate of change in bilayer capacitance is proportional to the strength of the applied stimulus (i.e. not the transmembrane voltage) and that dC/dt increases linearly with respect to the level of hair perturbation as given by airflow. Using the rms value of dC/dt, we also estimated the maximum percentage change in bilayer area for each airflow speed (details provided in supporting information). This was accomplished, by computing the amplitude of membrane capacitance during hair oscillation as given by:

$$C = \frac{1.3}{\sqrt{2}\,\omega_1}\left(\frac{\mathrm{d}C}{\mathrm{d}t}\right)_{\mathrm{rms}}, \qquad (2)$$

where, the ω_1 is the first natural frequency (180 Hz) of the hair determined from the PSDs of the sensing currents (figure 2(b)). The percentage change in the area is computed by dividing the amplitude of membrane capacitance by the capacitance of the membrane measured at zero volts. Because dC/dt is dependent only on airspeed, ω_1 does not vary with airflow speed, and the zero volts capacitance of the bilayer was constant in all tests, the computed percentage change in bilayer area is the product of a constant and the measured rms values of dC/dt. Thus, the corresponding percent changes in bilayer area versus airflow speed are provided on the right axis in figure 2(d).

The range of measured dC/dt values for the revised sensor is 0.8–6 nF s^{-1} across airflow speeds from 3 to 20 m s^{-1}, which is significantly higher than for the original sensor (45–60 pF s^{-1}) [1]. This increase in dC/dt values for the revised sensor is attributed to both higher levels of membrane bending and increased durability, which allows for measuring dC/dt at higher flow speeds. At the speeds tested, the measured values for dC/dt correspond to variations in membrane capacitance on the order of 0.2–2.0%, which is 10–100X higher than that measured for the initial membrane-based hair cell [1]. For example, the initial hair cell embodiment exhibited 0.027% area change at an approximate air speed of 7 m s^{-1} [1], whereas we measure a 0.68% change in area at the same air speed. Furthermore, at speeds nearing 20 m s^{-1}, the membranes exhibit changes in area of approximately 1.8%. These values for change in bilayer area agree well with critical areal strains of 1–5% measured elsewhere on phospholipid bilayers [21]. This increase in bilayer bending is attributed to fixing the base of the hair in the substrate, which creates a condition in which vibrational energy of the hair can be more effectively transmitted to the membrane, both through the aqueous volumes and indirectly through the substrate.

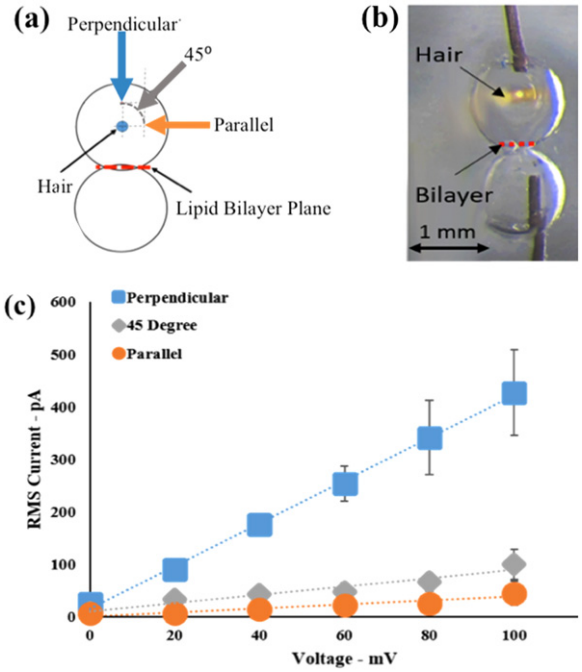

Figure 3. (a) Schematic of direction of airflow relative to membrane orientation and (b) corresponding picture of the hair cell in the same configuration shown in schematic. (c) Rms current versus direction of perturbation for steady airflow at 13.5 m s^{-1}.

4.1.2. Directionality of sensing response. While our prior work showed that the cause for changing membrane capacitance and current produced as a result of airflow is transverse bending of the membrane due to hair vibration [1], the effect of perturbation direction on the membrane's mechanoelectrical response has yet to be studied in detail. Thus, we characterized the sensing response of a membrane to airflow across the hair at angles of 0°, 45°, and 90° with respect to the planar lipid bilayer (figures 3(a) and (b)). At each angle, the rms current produced by airflow at 13.5 m s^{-1} and an applied voltage of 80 mV is measured as a function of applied voltage. Each data point in figure 3(c) shows the average of the rms current measured for three different membranes tested at each voltage and perturbation angle, and the error bars indicate ±1 standard deviation of the three responses. Here again, the area of each membrane is kept constant for all voltage levels and perturbation levels.

Similar to the data in figure 2(c), the data in figure 3(c) shows that the rms current increases linearly with increasing voltage, regardless of angle. However, the magnitude of the sensing current also depends on the angle of perturbation. Airflow across the hair in a direction perpendicular to the bilayer generates the largest response, while perturbations at angles more parallel to the membrane yield less current. Linear fits to the three current versus voltage series is used to compute the time rate change of capacitance at the different airflow directions. The values of R^2 for all linear fits are higher than 0.98. As shown in the previous section, the

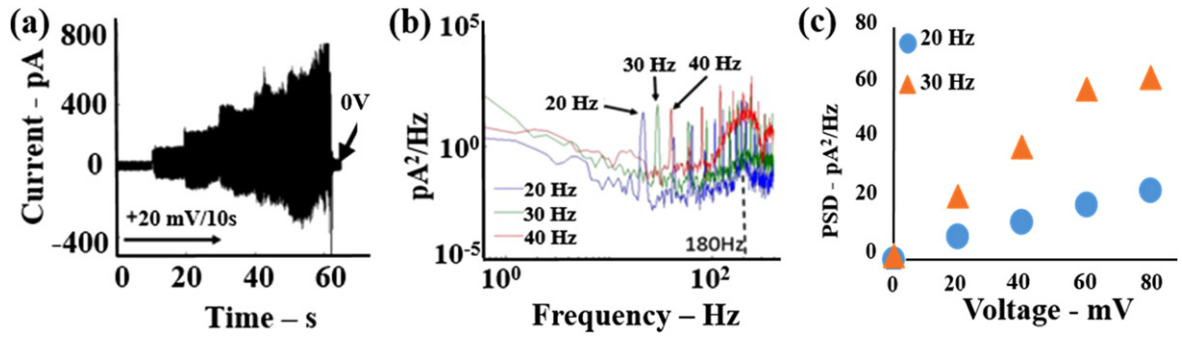

Figure 4. (a) The current response to 30 Hz oscillation applied to the hair by a shaker during which the voltage is increased by 20 mV every 10 s. (b) Frequency content of current responses for perturbation at 20, 30 and 40 Hz. (c) The magnitude of the PSD at the driving frequency versus voltage for 20 and 30 Hz driving frequencies.

bilayer moves at the same frequency regardless of airflow speed. A similar effect is observed here with respect to airflow direction, therefore the dt portion of the time rate change of capacitance is independent of the direction of airflow. Thus, we can conclude that changing the direction or strength of airflow only affects the capacitance of the membrane, the dC in dC/dt. The sensitivity value for perpendicular (90°) airflow is highest at 4.05 nF s^{-1}, whereas measured sensitivity is only 0.81 and 0.27 nF s^{-1} for 45° and parallel (0°) airflow, respectively. This result shows that the direction of the hair's motion directly influences the membrane's response to a particular perturbation. As the sensor is most sensitive when the hair is perturbed in a direction perpendicular to the membrane, this data provides added proof that transverse bilayer bending is responsible for the time rate change in capacitance. The fact that the raw currents measured for each direction of perturbation exhibit identical frequency responses (not shown) indicates that frequency of the membrane's motion is driven by oscillation of the hair and not the direction of applied airflow. Together, these results suggest that membrane-based hair cell sensors could be used to determine both the magnitude and direction of an applied stimulus.

4.1.3. Low frequency response. We also characterized the membrane response to stimuli at frequencies lower than the hair's resonance. In this set of tests, we used a mechanical shaker to vibrate the hair perpendicularly to the plane of the membrane (90°) at 20, 30, and 40 Hz. With this form of excitation, the horizontal displacement of the top of the hair decreases with increasing frequency because of power limitations that reduce the periodic displacement of the mechanical shaker. Shaker displacements for 20, 30 and 40 Hz frequencies were measured to be 2.5, 2.0 and 1.5 mm, respectively. The calculated values of hair deflection at the center of the excited droplet using a similar triangle approximation (i.e. minimal hair bending) are approximately 0.7, 0.6 and 0.5 mm, for 20, 30 and 40 Hz, respectively. Raw current in response to 30 Hz oscillation of the hair with about 2 mm deflection is shown in figure 4(a). The applied voltage is increased by 20 mV every ten seconds to 120 mV before being returned to zero as shown by the arrows. Here again, we see a voltage-dependent response in the measured current, which tells us that the current is generated by a time rate of change in the capacitance of the bilayer as the hair is continuously oscillated. Similar to free vibration or airflow tests that induce resonance in the hair (~180 Hz), this result confirms that the bilayer is capable of transducing motion of the hair at frequencies below resonance.

The PSDs of the current responses at the three oscillation frequencies at 60 mV are shown in figure 4(b), where the arrows indicate the first peak frequencies for the three current traces. For each oscillation setting, the frequency of this first peak matches the shaker (i.e. the hair) frequency. This result indicates that as the hair is being shaken in a direction perpendicular to the membrane, it produces a time rate change of capacitance in the membrane at the same frequency of the input excitation. The remaining peaks in the computed PSDs are found to be harmonic frequencies of the first peak of the current response. Also, there is a broad peak in the PSD of the current response for 40 Hz hair vibration close to the natural frequency of the hair, which is most likely due to detachment of the hair from the connecting rod that allows oscillation at the hair resonance frequency during the shaking.

Figure 4(c) shows the power distribution of the sensing current at 20 and 30 Hz, respectively, versus voltage. In this analysis the power generated by the positive electrode is taken out from each data points. As shown above with airflow, the power across the membrane generated by the time rate change of capacitance increases by increasing the applied voltage. We notice that higher driving frequency produces higher signal power. Because of this difference in sensor output at the two frequencies, we compare the ratio of time rate change of applied hair displacement, dx/dt, to the ratio of the measured rms current (equal to the ratio of the dC/dt at a given voltage) for both 20 and 30 Hz vibrations. The computed dx/dt ratio of the hair motion of 30–20 Hz $((dx/dt)_{30\ Hz}/(dx/dt)_{20\ Hz})$ is approximately 1.28. The average ratio of measured dC/dt for bilayer for 30–20 Hz $((dC/dt)_{30\ Hz}/dC/dt)_{20\ Hz})$ is 1.31 ± 0.12 for voltages between 20 and 80 mV. The fact that the ratio of the output (dC/dt) is within ±10% of the ratio of the input (dx/dt) at the two frequencies shows that the increased current produced at 30 Hz is due simply to the higher rate of change in the applied hair displacement. This

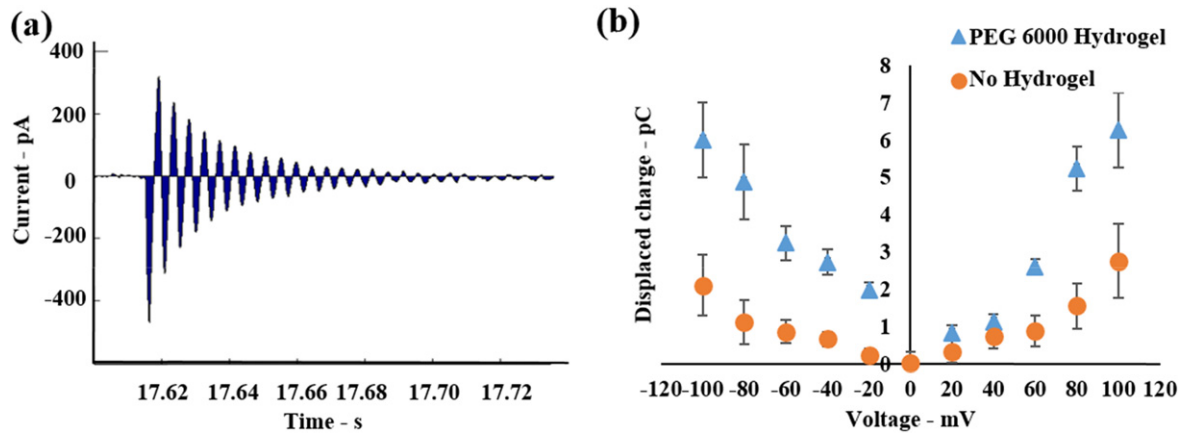

Figure 5. (a) Transient current response due to one flick of the hair (shaded area represents calculated displaced charge). (b) Displaced charge versus applied membrane voltage for bilayers formed between lipid-coated liquid volumes and photopolymerized PEG-hydrogels.

result also shows that the sensor exhibits a linear response in that the ratio of the output is equal to the ratio of the input at these frequencies. We did not consider the 40 Hz response in this comparison because the PSD of this measurement indicated that the hair likely detached from the shaker during excitation, which would cause the magnitude of response to not scale well with the applied frequency. Additionally, higher frequencies were not tested for the reason that the shaker displacement decreased significantly at higher driving frequencies.

4.1.4. Effect of aqueous volume composition. In the previous work, the lipid bilayer was formed between one lipid-encased liquid volume and one lipid-encased, water-swollen gel volume used to support the hair [1]. The fact that the PDMS substrate supports the hair in the new embodiment affords the use of either liquids or gel materials as the lipid-coated aqueous volumes. Thus, we now examine the effect of using liquid volumes or polymerized hydrogels as the aqueous volumes on the current response of the interfacial bilayer. Specifically, we form and characterize a membrane-based sensor consisting of two volumes of either liquid liposome solution or the hydrogel mixture. A bilayer is formed as described earlier, and, in the case of using gels, the hydrogel volumes are photopolymerized before characterization of sensing response. In place of airflow, sensing current is measured and recorded for 10 to 12 successive flicks of the hair using the automated flicker, each at applied voltages ranging from −100 to +100 mV in 20 mV intervals. In this set of experiments, the area of the bilayer in each test is not held constant. Therefore the bilayer area changes due to the electrowetting effect as we apply voltage across the membrane, and the current and displaced charges agrees with the third order model of the hair cell provided in equation (1).

Figure 5(a) shows a second-order underdamped current response of a single flick to the hair. To compare these transient responses for the two different aqueous compositions tested, we compute the total charge displaced across the membrane during hair vibration as the area under the current, versus time trace (shown as the shaded region). Figure 5(b) shows the average displaced charge across three separate membranes for each of the two aqueous compositions at varying applied voltages, where the error bars represent ±1 standard deviation. The data show that both compositions display a voltage-dependent charge response, where increasing the applied voltage results in a greater amount of displaced charge for the same flick. Moreover, we see that hydrogel-sandwiched membranes produce a larger response compared to bilayers formed between two liquid aqueous volumes. For example, a bilayer formed using liquid volumes generates a displaced charge of ∼4 pC at |100 mV|, while a bilayer formed between gel volumes generates nearly twice as much charge. The data show that charge for either case does not increase linearly with voltage, due to the fact that the area of the bilayer was not held constant in this experiment.

The slopes of linear fits to the displaced charge versus voltage data are extracted to compare the sensitivity of bilayer response for the two types of aqueous volumes. The observed sensitivity (0.066 pC mV^{-1}) for the bilayers formed between 10% PEG 6000 hydrogel is significantly higher than that (0.015 pC mV^{-1}) measured for a bilayer formed between aqueous volumes containing 0% gel. This value is the average absolute value of the slope of linear fits at both positive and negative voltages. The higher sensitivity of the hair cell sensor with bilayer formed between hydrogels indicates that the stiffer hydrogel materials on both sides of the membrane produce higher dC/dt in the membrane. While it may be counterintuitive, since a stiffer gel could possibly restrict bending of the bilayer, the hydrogels likely do a better job than liquid volumes at transmitting energy of the hair's motion to the interface. Instead, liquid volumes likely damp more energy, leading to a lower time rate of change in capacitance of the bilayer. Again, we noted that the membrane did not rupture due to flicking, even though it did rupture at high voltage. The durability of the membranes in both cases was similar in response to flicking.

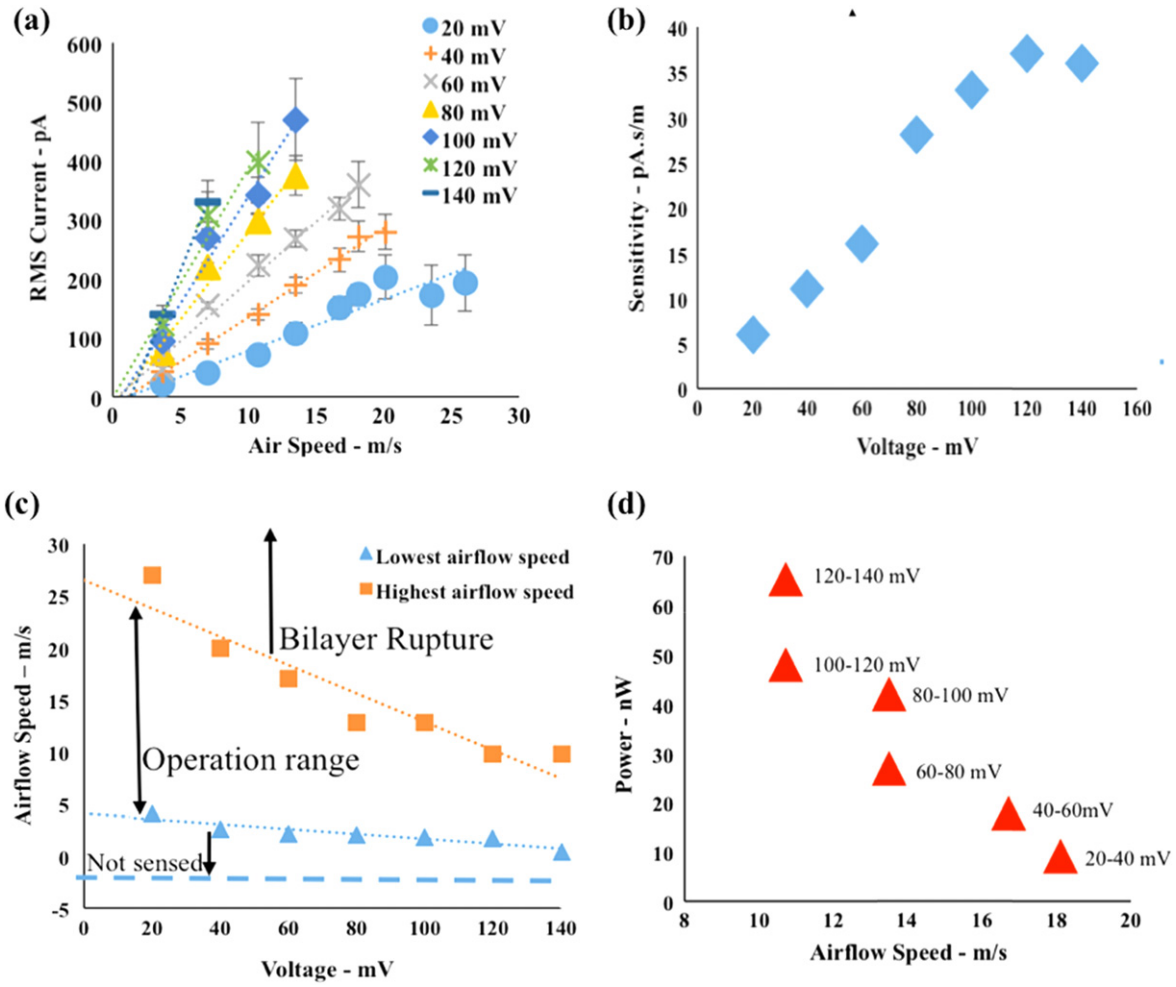

Figure 6. (a) Rms current versus airflow speed at different operation voltages. (b) Sensitivity to airflow at a direction perpendicular to the membrane versus voltage. (c) Minimum (triangles) and maximum (squares) airflow speeds that can be sensed versus operation voltage. (d) Electrical power of the membrane versus air speed at the maximum allowable voltage prior to rupture.

4.2. Quantification of sensor performance

The data presented thus far help explain the physical mechanism by which an interfacial lipid bilayer converts a mechanical stimulus into an electrical current. The effects of perturbation strength, direction, and frequency and aqueous volume composition on the magnitude and frequency content of the output current were studied. However, these tests also provide information useful for characterizing the assembly in terms of traditional sensor metrics including sensitivity, dynamic range, detection thresholds, and failure mechanisms.

Figure 6(a) re-presents the data from figure 2(c) in terms of sensor output (rms current) versus stimulus input (airflow across the hair in a direction perpendicular to the bilayer) at the tested values of membrane voltage. This format is structured specifically to examine the sensitivity, range, and threshold of the transduction process, instead of measuring dC/dt, where the applied voltage can be considered as a tunable operation point for the device. Similar to the current–voltage series, the current-airspeed data series show linear relationships across their operation ranges. The slopes of these series represent the sensitivities in response to airflow at various voltages (figure 6(b)). When only 20 mV is applied across the bilayer, the sensor exhibits a sensitivity of approximately 5 pA rms per m s^{-1} and can withstand airflow rates as high as 28 m s^{-1} before rupturing due to excessive mechanical perturbation. Conversely, an applied bias of 120 mV produces a much higher sensitivity (>35 pA rms per m s^{-1}) but across a narrower range of airspeeds (<15 m s^{-1}). This presentation confirms that sensitivity rises with increasing voltage, where the largest gain in sensitivity is observed between 20 and 100 mV.

The minimum current that the hair cell can sense is the interception of the linear fit of current versus airflow at different voltages and zero current (i.e. the x-axis) in figure 6(a). Both the minimum sensing threshold and the maximum allowable airflow speed of the sensor, as illustrated in figure 6(c), decrease with increasing applied voltage. For example, the minimum and maximum airflow speed at +20 mV are 4.2 and 28 m s^{-1}, respectively, whereas they fall to 0.6 and 13.5 m s^{-1}, respectively at +140 mV. Recalling the computed percent area changes of the membrane are functions of the stimulus level (figure 2(d)), these data provide insight into the amount of deformation and voltage that lead

to membrane rupture. An air speed of 13.5 m s^{-1} at 140 mV corresponds to a change in membrane area of roughly 1.3% (figure 2(d)), whereas biasing the membrane with only 40 mV allows for airflow at 18 m s^{-1} and 1.7% change in membrane area before rupture.

Using equation (S4), we computed the maximum electrical power of the membrane measured prior to rupture at each airflow speed (figure 6(d)) to understand if a common power level leads to membrane rupture. Instead, the data show that the maximum power in the membrane is a combination of both airspeed and voltage. At low applied voltages, a membrane can withstand higher airspeeds, and thus higher amounts of deformation, without rupturing. In contrast, the membrane is able to withstand much less perturbation from airflow when the applied bias is large. We see the maximum electrical power (~65 pW) of the membrane occurs for combinations of slower airflow and higher voltages across the different speeds, since the power is proportional to square of the applied voltage. Yet, for the range tested, neither airflow alone nor voltage was sufficient to cause membrane rupture. Thus, we conclude that both the applied voltage and the sustained perturbation level contribute to causing membrane failure, and that the mechanical energy state as opposed to the electrical power dissipated may provide a better marker of failure. One possibility is that voltage-induced electrostriction of the bilayer creates stored mechanical energy in the membrane that adds to the vibrational energy induced when the hair is perturbed.

5. Conclusion

Membrane-based hair cell sensors show capabilities for sensing both discrete and continuous types of perturbations. In this study, we showed that the current response of a revised membrane-based sensor is dependent on several parameters: (1) the voltage across the membrane, (2) the strength, direction, and frequency of the perturbation, and (3) the material compositions of the aqueous volumes used to form the bilayer. The revised embodiment features a hair that is rooted firmly in the polymeric substrate that also supports the lipid bilayer. Compared to the first generation membrane-based hair cell sensor, the results of these experiments show that the new embodiment is much more durable, allowing large and repeated deformations of the hair. Due to greater robustness, we were able to more fully characterize the mechanoelectrical transduction process of a membrane-based hair cell sensor. Cumulatively, the results confirm that the bilayer exhibits a time rate of change in capacitance (dC/dt) due to transverse bending in response to motion of the hair, where the magnitude of dC/dt depends on the strength and direction of the applied stimulus. Similar to the first generation of the hair cell sensor, analysis of the hair's motion relative to measured sensing currents at both resonance and lower frequency excitations show that the membrane vibrates at the same frequency of the hair. However, the higher values of dC/dt (0.8–6 nS s^{-1}) and percent change in membrane area (0.2–2.0%) indicate that cantilevering the hair in the solid substrate results in greater energy transfer to the membrane resulting in bending; this is likely due to both a stiffening effect of the hair and added transmission of energy through the substrate. A more subtle benefit of the revised embodiment is the fact that the lipid aqueous volumes can be either pure liquids or liquid-swollen gels material. Our tests on both types of volumes show that the freedom to vary the material composition can be used to tailor both the mechanical properties and sensitivity.

In context to its use as a sensor, this study yielded new information regarding the sensitivity and dynamic range of a membrane-based hair cell in response to airflow. These tests revealed that the current output by a sensor varies linearly with respect to the applied airflow for a given voltage level. However, a trade-off exists: while increasing the voltage amplifies the sensitivity of the response to airflow and reduces the minimum airflow speed that can be detected, it also narrows the range of airspeeds that can be detected without rupturing the bilayer. Nonetheless, the results confirm that the applied voltage can be used to tune the performance to a given application. A low voltage <60 mV may be best suited for sensing airflow across a wide range of speeds, while increasing the applied voltage to ~100 mV can provide greater sensitivity and a lower threshold for detecting slower sources of airflow. This finding is especially important when comparing sensor modalities and in configuring a membrane-based sensor for a specific sensing application.

Acknowledgments

The authors are grateful for funding provided by the National Science Foundation (CMMI, Sensors and Sensing Systems Award: 1129951).

References

[1] Sarles S A, Madden J D W and Leo D J 2011 Hair cell inspired mechanotransduction with a gel-supported, artificial lipid membrane *Soft Matter* **7** 4644–53
[2] Brownell W, Bader C, Bertrand D and de Ribaupierre Y 1985 Evoked mechanical responses of isolated cochlear outer hair cells *Science* **227** 194–6
[3] Flock Å, Flock B and Murray E 1977 Studies on the sensory hairs of receptor cells in the inner ear *Acta Oto-laryngologica* **83** 85–91
[4] Barth F 1998 *Comparative Hearing: Insects* ed R Hoy *et al* (New York: Springer) pp 228–78
[5] Devarakonda R, Barth F G and Humphrey J A C 1996 Dynamics of arthropod filiform hairs: IV. Hair motion in air and water *Phil. Trans. R. Soc.* B **351** 933–46
[6] Abdulsadda A T and Tan X 2012 An artificial lateral line system using IPMC sensor arrays *Int. J. Smart Nano Mater.* **3** 226–42
[7] Dagamseh A, Lammerink T, Kolster M, Bruinink C, Wiegerink R and Krijnen G 2010 Dipole-source localization using biomimetic flow-sensor arrays positioned as lateral-line system *Sensors Actuators* A **162** 355–60

[8] Park B K and Lee J S 2012 Dynamic behavior of flexible sensory hair in an oscillating flow *J. Mech. Sci. Technol.* **26** 1275–82
[9] Hein M A, Maqableh M M, Delahunt M J, Tondra M, Flatau A B, Shield C K and Stadler B J 2013 Fabrication of bioinspired inorganic nanocilia sensors *IEEE Trans. Magnetics* **49** 191–6
[10] Masoud H and Alexeev A 2011 Harnessing synthetic cilia to regulate motion of microparticles *Soft Matter* **7** 8702
[11] Rizzi F, Qualtieri A, Dattoma T, Epifani G and De Vittorio M 2015 Biomimetics of underwater hair cell sensing *Microelectron. Eng.* **132** 90–7
[12] Qualtieri A, Rizzi F, Todaro M, Passaseo A, Cingolani R and De Vittorio M 2011 Stress-driven AlN cantilever-based flow sensor for fish lateral line system *Microelectron. Eng.* **88** 2376–8
[13] Hudspeth A J and Corey D P 1977 Sensitivity, polarity, and conductance change in the response of vertebrate hair cells to controlled mechanical stimuli *Proc. Natl Acad. Sci.* **74** 2407–11
[14] Crawford A C and Fettiplace R 1980 The frequency selectivity of auditory nerve fibres and hair cells in the cochlea of the turtle *J. Physiol.* **306** 79–125
[15] Roberts W, Jacobs R and Hudspeth A 1990 Colocalization of ion channels involved in frequency selectivity and synaptic transmission at presynaptic active zones of hair cells *J. Neurosci.* **10** 3664–84
[16] Brundin L, Flock A and Canlon B 1989 Sound-induced motility of isolated cochlear outer hair cells is frequency-specific *Nature* **342** 814–6
[17] Sarles S A and Leo D J 2010 Regulated attachment method for reconstituting lipid bilayers of prescribed size within flexible substrates *Anal. Chem.* **82** 959–66
[18] Hwang W L, Chen M, Cronin B, Holden M A and Bayley H 2008 Asymmetric droplet interface bilayers *J. Am. Chem. Soc.* **130** 5878–9
[19] Sarles S A, Stiltner L J, Williams C B and Leo D J 2010 Bilayer formation between lipid-encased hydrogels contained in solid substrates *ACS Appl. Mater. Interfaces* **2** 3654–63
[20] Tamaddoni N and Sarles S A 2013 Characterizing the sources of current generated by a membrane-based hair cell sensor *ASME 2013 Conf. on Smart Materials, Adaptive Structures and Intelligent Systems SMASIS* **2013** 3141
[21] Needham D and Nunn R S 1990 Elastic deformation and failure of lipid bilayer membranes containing cholesterol *Biophys. J.* **58** 997